

Vesta's UV Lightcurve: Hemispheric Variation in Brightness and Spectral Reversal

Amanda R. Hendrix

Jet Propulsion Laboratory

Mail Stop 230-250

4800 Oak Grove Dr.

Pasadena, CA 91109

hendrix@jpl.nasa.gov

ph. (818)393-1628

fax (818)393-4669

Faith Vilas

NASA Johnson Space Center

Michel C. Festou

Observatoire Midi-Pyr'en'ees, Toulouse, France

29 pages

4 figures

2 tables

proposed running head: Vesta's UV Spectral Reversal

correspondence address: Amanda Hendrix

Jet Propulsion Lab

M/S 230-250

4800 Oak Grove Dr.

Pasadena, CA 91109

Abstract.

Spectra of asteroid 4 Vesta obtained in October 1990 with the International Ultraviolet Explorer are reanalyzed and reinterpreted. A large portion of the eastern hemisphere (based on the prime meridian definition of Thomas *et al.*, 1997a) is darker at UV wavelengths than much of the western hemisphere. The UV lightcurve is in contrast with the visible lightcurve, which shows that the eastern hemisphere is brighter than the western. These IUE spectra of Vesta thus may be evidence for the “spectral reversal,” first seen on the Moon by Apollo 17, where the visibly brighter lunar highlands are darker than the maria at far-UV wavelengths.

We investigate Vesta’s UV lightcurve and spectral reversal. We model the UV spectra using laboratory spectra of howardite and diogenite meteorites, as well as using candidate materials (pyroxenes) based on knowledge of Vesta’s composition from visible and near-infrared spectroscopy. Only the models using the meteorite spectra result in a spectral reversal, and we conclude that space weathering on Vesta (particularly on the older, more weathered western hemisphere) is manifested in brightening the surface at ultraviolet wavelengths, even as it darkens the surface at visible wavelengths. This is likely because grain acquire a weathering coating to which shorter wavelengths are more sensitive.

Keywords: Asteroids, Vesta

Ultraviolet Observations

Surfaces, Asteroids

Introduction.

Vesta is a distinctive asteroid due to its basaltic composition, and because it is known to be compositionally variable across its surface (Gaffey, 1997). Vesta is also known to be the parent body of the howardite, eucrite and diogenite (HED) meteorites (McCord *et al.*, 1970; Binzel and Xu, 1993).

Binzel *et al.* (1997) produced a geologic map of Vesta based on HST images, which is largely consistent with the mineralogical map derived by Gaffey (1997) from ground-based telescopic spectra. The entire body, including the western hemisphere, is dominated by Fe-rich and Ca-rich pyroxenes similar to eucrite and howardite meteorites. The eastern hemisphere has contributions from Mg-rich and Ca-poor pyroxenes, similar to diogenite meteorites, in addition to olivine. The results of Cochran and Vilas (1998) indicate that augite (high-Ca pyroxene) is the dominant pyroxene on Vesta, based on the shape of the 506.5 nm feature. The surface of the western hemisphere is thought to be old, while the eastern hemisphere consists of fresher units that may have been exposed through impact (Gaffey, 1997). The topographic map of Thomas *et al.* (1997b), produced from 1996 WFPC2 images in combination with 1994 images, may be consistent with this idea of hemispheric age variation. The northern hemisphere is overall smoother than the southern hemisphere; the eastern hemisphere (particularly in the south) is dominated by topographic highs and lows. The western hemisphere, while containing topographic variations, also consists of a relatively large region of topographic average height. This region may represent the oldest terrain on Vesta, unaltered by impact.

Thomas *et al.* (1997a) refined the shape and spin pole of Vesta, and proposed a new definition of prime meridian (from which an eastern and a western hemisphere can be defined; see below) based on the location of the spot "Olbers," a 200 km region of relatively low albedo in Hubble Space Telescope (HST) WFPC2 images (Zellner *et al.*, 1997). The radii of Vesta were measured at 289, 280, 229 \pm 5 km (Thomas *et al.*, 1997a).

In light of the recent HST measurements of composition, topography and shape, as well as Gaffey's 1997 model of Vesta's mineralogical variations, we present here the results of a re-analysis of high quality observations obtained in 1990 with the International Ultraviolet Explorer (IUE) by Festou *et al.* (1991), and we report the detection of UV spectral variations across the surface and a spectral reversal on Vesta. We explore possible causes of the UV lightcurve, including topographic and compositional variations and discuss the relationship with space weathering effects.

IUE Observations of Vesta.

The IUE observations of Vesta were performed in October 1990 and are discussed by Festou *et al.* (1991). Sixteen spectra were taken with the Long Wavelength Prime (LWP) spectrograph which covers the 1900-3400 Å wavelength range; details of the observations are outlined in Table I. In this analysis, we use IUE Newly-Extracted Spectra (INES) processed data files. These files benefit from an improved geometric correction, a more accurate photometric correction and an increased signal-to-noise ratio of the extracted IUE data through the use of new processing algorithms (ref. ESA SP 413). The observations were performed over a period of 12 hours, which covers more than two Vesta rotations, based on a rotational period of 5.342 hours (Drummond *et al.*,

1988). During the observations, the solar phase angle was 17° . Vesta was 1.76 AU from Earth and 2.54 AU from the Sun. We can determine the sub-Earth latitude and longitude during the 1990 observations by using the new definition of prime meridian given by Thomas *et al.* (1997a):

$$W = 292^\circ + 1617.332776d$$

where d is the number of days from the standard epoch of 2000 January 1.5. Using the spin axis position from Thomas *et al.* (1997a) of 301° RA and 41° Dec and the RA and Dec of Vesta during the IUE observations (RA \sim 4 hr, Dec 11°), we find that the sub-Earth latitude was $\sim 13^\circ$ S.

A Revised UV Lightcurve: Spatial Variations in UV Brightness.

Figure 1 displays the measured flux at several wavelengths versus longitude. The lightcurves are similar to those displayed in Festou *et al.* (1991), but plotted vs. longitude rather than vs. phase. (Festou *et al.* plotted phase curves over slightly different wavelength bands.) The lightcurves display error bars, which are computed by the optimal extraction algorithm in the INES processing pipeline. The noise in the IUE data is determined after a complex procedure has been applied to the raw data. An error is associated to each pixel. Since our results represent average quantities calculated from numerous spectral and spatial pixel values, the individual errors are treated like Poissonian errors. We note a significant improvement in the accuracy of the spectral albedo in comparison to results obtained by Festou *et al.* (1991) using the old software.

Using the reprocessed data, it is clear that spatial variations in brightness are present. A hemispheric dichotomy is most noticeable at $\sim 2900\text{-}3000 \text{ \AA}$, where the flux variations are larger than the error bars. The eastern hemisphere of Vesta, particularly the $[0, -90^\circ]$ region, is darker than the western hemisphere.

The most likely sources of a lightcurve of any asteroid are the shape of the asteroid or large-scale hemispheric compositional variations. We also note that a hemispheric variation in amount of space weathering, which would be due to one hemisphere being geologically younger (due to geologic activity or the occurrence of large-scale cratering, which exposes fresher underlying material) could affect the lightcurve in that space weathering tends to spectrally modify material.

It is known that Vesta's visible lightcurve is due to albedo variations rather than shape (Gradie *et al.*, 1978; Binzel *et al.*, 1997; Zellner *et al.*, 1997). The long axis is viewed at longitudes 60° and 240°W , while the visible lightcurve maximum occurs at 260° and the minimum occurs at 60°W . This lack of coordination between the shape model and visible lightcurve is evidence that the UV lightcurve of Fig. 1c is not due to Vesta's shape. In the next sections, we explore the other possible explanations of the UV lightcurve, including variations in composition and amounts of space weathering across the surface. We refer to Table II, which summarizes the large-scale relative differences between Vesta's two hemispheres.

Figure 1c reveals not only that Vesta displays a UV lightcurve, but that the UV lightcurve is offset from the visible lightcurve. Vesta's western hemisphere is brighter in the UV, and darker at visible wavelengths, than the eastern hemisphere. Such a spectral reversal has been observed previously only on the Moon.

Vesta's Spectral Reversal

The fact that Vesta's UV lightcurve is offset by almost 180° from the visible lightcurve means that this asteroid displays a spectral reversal, a phenomenon seen before on the Moon and lunar samples. The lunar spectra reversal was first reported by Lucke *et al.* (1974) using Apollo 17 UVS measurements, where it was noted that the visibly dark lunar maria are 5-10% brighter than the highlands at far-UV wavelengths (1470 Å). Henry *et al.* (1976) explain the lunar spectral reversal as being due to the higher index of refraction of mare material relative to highlands material. The index of refraction of many materials increases with decreasing wavelength, so that they become brighter at shorter wavelengths. This is important because at shorter wavelengths, surface scattering dominates over volume scattering so that reflectance is directly related to the index of refraction (Henry *et al.*, 1976). However, Henry *et al.* (1976) also note that the correlation between visibly bright and UV-dark lunar regions is imperfect, and that UV spectra may therefore contain further information than what is known from visible spectra. In particular, since far-UV radiation is less penetrating than visible radiation, short wavelengths are more sensitive to thin coatings on grains that may be the result of weathering processes (Lucke *et al.*, 1974).

Wagner *et al.* (1987) measured UV-IR spectra of many materials and found the transition between reflectance dominated by volume-scattering and reflectance dominated by surface scattering to occur between 150 and 450 nm, depending on the material. The Galileo UVS measured the moon in the same wavelength (2100-3200Å) range at which Vesta was measured by IUE. At these near-UV wavelengths, the lunar highlands are

brighter than the maria (Hendrix, 1996), although the difference in brightness decreases with wavelength (i.e., the ratio of the spectral reflectance of the maria to the highlands is blue). The lunar spectral reversal therefore likely occurs somewhere between 1470 Å and 2100 Å, in agreement with Wagner's lab measurements of lunar samples, which show the lunar spectral reversal occurring usually between 1700 and 2000 Å. Vesta's spectral reversal must occur longward of 3200 Å, since the IUE data show that the UV lightcurve is opposite that in the visible. Thus, on Vesta, the spectral reversal occurs at a longer wavelength than on the Moon. Indeed, Wagner's lab spectra of diogenite and howardite indicate that longward of ~3000 Å diogenite is brighter than howardite, but the opposite is true shortward of 3000 Å.

Vesta's UV Spectra: Compositional Modeling.

The compositional map produced by Gaffey (1997) and shown on the new longitude scale by Binzel *et al.* (1997) indicates large-scale variations between Vesta's two hemispheres. The western hemisphere includes pyroxenes similar to eucrite and/or howardite meteorites, while the eastern hemisphere is a combination of pyroxenes similar to eucrite and/or howardite meteorites, plus a mixture of pyroxenes similar to diogenite meteorites, plus olivine (Table II).

In light of this knowledge of Vesta's composition, we modeled Vesta's eastern and western hemisphere spectra to see if combinations of pyroxenes, olivines and meteoritic material could account for hemispheric UV variations and the spectral reversal. We note that very few UV laboratory spectra of candidate materials exist, so we

did not have many options for models, but we expect that the results should give an indication of the feasibility of the method and idea.

To determine Vesta's ultraviolet reflectance, we divide the IUE flux by the SOLSTICE-measured solar spectrum (Rottman *et al.*, 1993):

$$\text{reflectance} = F_V \cdot R^2 \cdot \Delta^2 / F_S \cdot r^2$$

where F_V is the flux from Vesta, F_S is the solar flux, R is the Vesta-Sun distance, Δ is the Earth-Vesta distance, and r is Vesta's equivalent radius (266 km). Here we do not attempt to correct for phase angle. Since all observations were performed at 17° solar phase angle, it is not necessary to correct for phase angle to intercompare the observations. Thus, the spectra that we model represent Vesta's UV reflectance at 17° phase rather than the geometric albedo. Resultant reflectance spectra are shown in Fig. 2a for two observations. When dividing by the solar spectrum, in some Vesta spectra, there are residual features, particularly around 2800 and 2850 Å. These are artifacts likely due to movement of the asteroid within the slit during the observation, as discussed by Festou *et al.* (1991).

To model Vesta's reflectance, we used laboratory spectra from the two primary sources of UV laboratory data, Wagner *et al.* (1987) and the USGS Spectroscopy Laboratory (Clark *et al.*, 1993). We used a two component model:

$$\text{model} = A \cdot (x \cdot R_1 + (1-x) \cdot R_2)$$

where R_1 and R_2 are the reflectance spectra of the candidate materials, x is the amount of R_1 (0-100%), and A is a scaling factor. We also tried a three-component model, where olivine was the third component, at no more than 10%. For each combination of candidate materials, we determined the values of A and x that best fit the UV spectra, and then checked whether the outcome was feasible based on what is known from the visible.

From the USGS Spectral Library, we tried using spectra of nine pyroxenes (bronzite, enstatite, three diopsides, acmite, fassaite, and two augites). The USGS Spectral Library also included the spectra of seventeen olivines, which we modeled in varying combinations with the pyroxenes. From the Wagner *et al.* (1987) data set, we tried spectra of 5 pyroxenes (aubrite, enstatite, diopside, hedenbergite and augite), 2 olivines (fayalite and forsterite) and 2 meteorites with Vesta as a likely origin (Johnstown diogenite and Bununu howardite).

We focussed on the Wagner data set, as we obtained no satisfactory models of the UV Vesta spectra using the USGS reflectance spectra. Using the Wagner laboratory data, we tried combinations of all materials, setting an upper limit of 10% to any olivine included in the model. Using the non-meteorite material, we obtained satisfactory fits to the UV spectra of Vesta (Fig. 2a). The best fit was obtained using a combination of aubrite (83%) and enstatite (17%) for the western hemisphere and 90% aubrite plus 10% fayalite for the eastern hemisphere. Such models correspond with what is known about Vesta's composition from visible and near-IR spectroscopy (Table II). However, this model does not account for Vesta's spectral reversal. As shown in Fig. 2b, the model of the western hemisphere is brighter at UV wavelengths, and continues to be brighter than

the eastern hemisphere, even at visible wavelengths where it is known that the eastern hemisphere is brighter.

Using the meteorite material (plus olivine), we found a combination of materials that fit the UV spectra adequately and also demonstrated a spectral reversal such as we might expect on Vesta; the models are shown in Fig 3a. The eastern hemisphere was fit with a combination of 54% howardite, 36% diogenite and 10% fayalite. The western hemisphere was fit with 90% howardite and 10% diogenite. The models are concurrent overall in terms of what is known to be present on Vesta's surface from visible spectroscopy (Table II). Both hemispheres are dominated by howardite/eucrite-type materials, but the eastern hemisphere also has some small amount of olivine (10% according to Gaffey) and some amount of diogenite-type material. The western hemisphere may not contain a large amount of diogenite (Gaffey) but we found it was necessary to better fit the UV spectrum (in particular, to make the spectrum as red as it is). The magnitude of the variation in hemispheric brightness at visible wavelengths is also concurrent with what has been reported (REF Gaffey, etc.)

The fact that our models that use non-meteoritic samples do not result in a spectral reversal, while those that use samples of HED meteorites do, suggests that the spectral reversal is related to exposure to the space environment. This is consistent with the Wagner *et al.* (1987) laboratory data that show the lunar spectral reversal only in spectra of lunar soils (more weathered), not in spectra of powdered rocks (less weathered). We thus contend that Vesta's UV spectra and spectral reversal can be explained using meteorite spectra better than mineral spectra because the meteorites have

undergone some amount of space weathering that has affected the surfaces of the grains, to which UV spectroscopy is sensitive.

The Effects of Space Weathering

Global Effects of Space Weathering on Vesta

Space weathering, the bombardment of airless bodies by micrometeoroids and irradiation by solar wind particles, affects solar system bodies by darkening and reddening their surfaces, as well as degrading absorption features (Chapman, 1996). These effects, particularly in the visible and near-IR, are well documented for the Moon (e.g., Pieters *et al.*, 1993), where powdered rock samples are spectrally different from spectra of the lunar soil. The precise effect of weathering may be the production of nanophase iron coating the particles, produced by vapor deposition. The ferrous silicate vapor deposition production necessary for this process to coat particles and darken and redden the surface is solar wind irradiation (Hapke, 2000).

In the ultraviolet, lunar space weathering effects are less clear, but may be similar to those seen at longer wavelengths. Laboratory spectra of lunar soils (Wagner *et al.*, 1987) exhibit ultraviolet reflectance spectra (shortward of 300 nm) that are darker (and may have fewer spectral features) than the reflectance spectra of powdered lunar rocks. As previously stated, the spectra of lunar soils exhibit a spectral reversal, while the spectra of powdered lunar rocks do not.

In the asteroid belt, fewer studies of space weathering effects have been performed than for the moon. Matson *et al.* (1977) pointed out that asteroids do not exhibit the red spectral reflectances of the Moon and Mercury, although they are also

airless bodies and thus should be similarly affected by weathering processes. They concluded that the difference could be attributed to the asteroids' compositions, and/or the lower impact velocities experienced by asteroids. More recently, however, weathering has been proposed as the source of spectral differences between ordinary chondrite (OC) meteorites and their proposed parent bodies, S-class asteroids (Chapman, 1996; Hapke, 2000). Hapke (2000) finds that the addition of nanophase Fe-bearing coatings to the grains of an OC meteorite sample results in spectral features similar to those of an S-type asteroid. Although the solar wind flux is lower in the asteroid belt than at the Moon, Hapke argues that less nanophase Fe is required to produce weathering effects on asteroids. Furthermore, on two S-type asteroids, Gaspra (semi-major axis $a=2.2$ AU) and Ida ($a=2.95$ AU), Galileo SSI camera data indicate that a number of small, relatively fresh craters are blue compared with the reddish rest of the surface, using the $0.4/0.56 \mu\text{m}$ ratio, and exhibit stronger $1 \mu\text{m}$ absorption bands (Helfenstein *et al.*, 1994; Chapman, 1996). These Galileo and laboratory results indicate that weathering does indeed occur in the asteroid belt and its effects can be analogous to those on the Moon.

Because Vesta is known to be spectrally similar to HED meteorites at visible/IR wavelengths (McCord *et al.*, 1970), whereas S-type asteroids are spectrally different than ordinary chondrite meteorites, Vesta may respond differently to space weathering than S-type asteroids. Although Vesta may not display the "standard" effects of space weathering at visible wavelengths, the UV data indicate that it does exhibit a spectral reversal which on the moon seems to be related to space weathering. This UV spectral reversal may therefore be an important indicator of exposure, regardless of the effects of weathering at longer wavelengths.

Hemispheric Variations in Space Weathering on Vesta

Recent HST results may suggest hemispheric variations in space weathering effects on Vesta ($a=2.54$ AU). Binzel *et al.* (1997) show that Vesta's $1 \mu\text{m}$ band is deeper, indicative of fresher material, on the eastern hemisphere. Furthermore, western hemisphere regions display an decreased albedo and band depth ratio compared with eastern hemisphere regions; space weathering is one process that may bring about this effect. The authors conclude that, if these albedo-band depth variations are due to space weathering, western hemisphere regions have existed over the age of the solar system.

A topographic map of Vesta (Thomas *et al.*, 1997b), produced from HST images, displays excursions in altitude up to ± 12 km compared to the reference ellipsoid and is reproduced in Fig. 3a. Figure 3b shows the topographic map projected onto Vesta's shape model, viewed at different central longitudes looking at 20°S (similar to the IUE viewing geometry of 13°S). The northern hemisphere is topographically somewhat smoother than the southern hemisphere, which is apparently dominated by a large impact feature near 60°S and the surrounding accumulation of excavated material. The eastern hemisphere (longitudes $180\text{-}360^\circ$, right side of Fig. 3a) appears to vary more drastically in topography than the western hemisphere. Over the majority of the western hemisphere, the most drastic change in elevation is 12 km, while the eastern hemisphere is dominated by a topographic variation of 24 km. This is consistent with the idea that the western hemisphere of Vesta is dominated by old crustal material (Gaffey, 1997), while the eastern hemisphere has apparently been reworked by impact, creating topographic variations and revealing compositional differences (see Table II).

A global comparison between the HST topographic map (Fig. 3b) and the IUE-derived lightcurve of Fig. 1c suggests that the UV-dark region corresponds to the “fresher” overturned material related to the south-pole crater, in particular, the crater rim near 20°S, 320-350°W. Correspondingly, the UV-bright western hemisphere is dominated by a large region of mean height (yellow in the topographic map), suggesting this region has not been affected by impact or accumulation of material after impact. This material is thus likely older than the exposed topographically low and high places, and may thus have experienced more weathering processes. We suggest that Vesta’s spectral reversal, and relative UV brightness of the older western hemisphere, are due to the longer exposure time of this region, allowing it to accumulate more coatings (possibly nano-phase iron as suggested by Hapke) that result in greater reflectance due to surface scattering at UV wavelengths.

Conclusions.

In an analysis of reprocessed IUE data of Vesta, we find that Vesta exhibits spatial variations in UV brightness: the western hemisphere is brighter than the eastern hemisphere. This is in contrast with the visible lightcurve which shows that Vesta’s eastern hemisphere is brighter than the western. We have modeled Vesta’s UV spectra with both laboratory spectra of candidate pyroxenes and olivines, as well as with laboratory spectra of howardite and diogenite meteorites. The UV spectra do not contain any significant spectral features so the model fits are non-unique. However, the fits using non-meteorite samples do not produce a spectral reversal, while those using the meteorite spectra do. We suggest that, as on the Moon, Vesta’s spectral reversal is due to space

weathering processes over the age of the asteroid. We suggest that Vesta's older eastern hemisphere is relatively bright in the UV because of its greater amount of exposure compared to the western hemisphere, which experienced a large impact and associated overturning of surrounding material. The grains of the eastern hemisphere likely have accumulated more exposure-related coatings to which UV spectroscopy is more sensitive than is visible spectroscopy. The coatings result in greater reflectance due to an increase in surface scattering.

Acknowledgements

This work was performed while ARH was at University of Colorado's Laboratory for Atmospheric and Space Physics, and was a NASA-ASEE Summer Faculty Fellow at Johnson Space Center, and with the support of a Johnson Space Center Director's Grant. FV acknowledges support from the NASA Planetary Astronomy program. Many thanks to Peter Thomas for providing Vesta topographic maps, and to Mike Gaffey for the sub-Earth latitude-determination scheme.

References.

Proceedings of the last IUE Conference: ESA SP 413.

Binzel, R. P., M. J. Gaffey, P. C. Thomas, B. H. Zellner, A. D. Storrs, E. N. Wells
1997. Geologic mapping of Vesta from 1994 Hubble Space Telescope images.

Icarus **128**: 95-103.

Binzel, R. P. and S. Xu 1993. Chips off of asteroid 4 Vesta: Evidence for the parent
body of basaltic achondrite meteorites. *Science* **260**: 186-191.

Calvin, W. M., R. N. Clark, R. H. Brown, J. R. Spencer 1995. Spectra of the Icy
Galilean Satellites from 0.2 to 5 μm : A Compilation, New Observations, and a
Recent Summary. *JGR* **100**: 19041-19048.

Chapman, C. R. 1996. S-type asteroids, ordinary chondrites, and space weathering: The
evidence from Galileo's fly-bys of Gaspra and Ida. *Meteoritics and Planetary
Science* **31**: 699-725.

Clark, R.N., G.A. Swayze, A. Gallagher, T.V.V. King, and W.M. Calvin 1993. The U.
S. Geological Survey, Digital Spectral Library: Version 1: 0.2 to 3.0 5μ , U.S.
Geological Survey, Open File Report 93-592, 1340 pages, 1993 (online at:
<http://speclab.cr.usgs.gov>).

Cochran, A. L. and F. Vilas 1998. The changing spectrum of Vesta: Rotationally
resolved spectroscopy of pyroxene on the surface. *Icarus* **134**: 207-212.

Drummond, J., A. Eckart, E. K. Hege 1988. Speckle interferometry of asteroids. IV.
Reconstructed images of 4 Vesta. *Icarus* **73**: 1-14, 1988.

- Festou, M. C., S. A. Stern, G. P. Tozzi 1991. Asteroid 4 Vesta: Simultaneous visible and ultraviolet IUE observations. *Icarus* **94**: 218-231.
- Gaffey, M. J. 1997 "Surface lithologic heterogeneity of asteroid 4 Vesta. *Icarus* **127**: 130-157.
- Gradie, J., E. Tedesco, B. Zellner 1978. Rotational variation in the optical polarization and reflection spectrum of Vesta (abstract). *Bull. Amer. Astron. Soc.* **10**: 596.
- Hapke, B. 2000. How to turn OC's into S's: Space weathering in the asteroid belt. In *Lunar and Planetary Science XXXI*, Abstract#1087, Lunar and Planetary Institute, Houston (CD-ROM), 2000.
- Helfenstein, P., J. Veverka, P. C. Thomas, D. P. Simonelli, P. Lee, K. Klaasen, T. V. Johnson, H. Breneman, J. W. Head, S. Murchie, F. Fanale, M. Robinson, B. Clark, J. Granahan, H. Garbeil, A. S. McEwen, R. L. Kirk, M. Davies, G. Neukum, S. Mottola, R. Wagner, M. Belton, C. Chapman, C. Pilcher 1994. Galileo photometry of asteroid 951 Gaspra. *Icarus* **107**: 37-60.
- Hendrix, A. R. 1996. *The Galileo Ultraviolet Spectrometer: In-Flight Calibration and Ultraviolet Albedos of the Moon, Gaspra, Ida and Europa*. Ph.D. thesis, University of Colorado.
- Henry, R. C., W. G. Fastie, R. L. Lucke, B. W. Hapke 1976. A Far-Ultraviolet Photometer for Planetary Surface Analysis. *Moon* **15**: 51-65.
- Lucke, R. L., R. C. Henry, W. G. Fastie 1974. Far-Ultraviolet Lunar Mapping From Apollo 17 (abstract). *Lunar Science V* p. 469, Lunar Science Institute, Houston.
- Matson, D. L., T. V. Johnson, G. J. Veeder 1977. Soil maturity and planetary regoliths: The Moon, Mercury, and the asteroids. *Proc. Lunar Sci. Conf.* **8**: 1001-1011.

- McCord, T. B., J. B. Adams, T. V. Johnson 1970. *Science* **168**: 1445.
- Pieters, C. M., E. M Fischer, O. Rode, A. Basu 1993. Optical effects of space weathering: The role of the finest fraction." *J. Geophys. Res.* **98**: 20817-20824.
- Rottman, G. J., T. N. Woods, T. P. Sparn 1993. Solar-Stellar Irradiance Comparison Experiment 1 1. Instrument design and operation. *J. Geophys. Res.* **98**: 10667-10677.
- Thomas, P. C., R. P. Binzel, M. J. Gaffey, B. H. Zellner, A. D. Storrs, E. Wells 1997a. Vesta: Spin pole, size, and shape from HST images. *Icarus* **128**: 88-94.
- Thomas, P. C., R. P. Binzel, M. J. Gaffey, A. D. Storrs, E. N. Wells, B. H. Zellner 1997b. Impact excavation on asteroid 4 Vesta: Hubble Space Telescope results. *Science* **277**: 1492-1995.
- Wagner, J. K., B. W. Hapke, E. N. Wells 1987. Atlas of reflectance spectra of terrestrial, lunar and meteoritic powders and frosts from 92 to 1800 nm. *Icarus* **69**: 14-28.
- Zellner, B. H., R. Albrecht, R. P. Binzel, M. J. Gaffey, P. C. Thomas, A. D. Storrs, E. N. Wells 1997. Hubble Space Telescope images of asteroid 4 Vesta in 1994. *Icarus* **128**: 83-87.

Table I. IUE Observations of Vesta^a

Observation	Time (UT)	Sub-Earth Longitude
LWP 18949	15:18	156.5°
LWP 18950	16:01	205.3° (-154.7°)
LWP 18951	16:46	256.2° (-103.8°)
LWP 18952	17:32	307.5° (-52.5°)
LWP 18953	18:14	355.1° (-4.9°)
LWP 18954	18:59	45.3°
LWP 18955	19:40	92.0°
LWP 18956	20:32	149.8°
LWP 18957	21:28	212.7° (-147.3°)
LWP 18958	22:17	268.8° (-91.2°)
LWP 18959	23:07	324.2° (-35.8°)
LWP 18960	23:59	19.2°
LWP 18961	00:47	76.8°
LWP 18962	01:34	130.1°
LWP 18963	02:24	185.5° (-174.5°)
LWP 18964	03:12	240.1° (-119.9°)

^a All observations were performed on October 6-7, 1990; sun-Vesta distance of 2.54 AU, Earth-Vesta distance of 1.76 AU; phase angle of 17°.

Table II. Summary of Vesta's Hemispheric Differences

Note: this table represents large-scale differences between the two hemispheres

WEST	EAST
geologically old	geologically young
more level topographic regions	more variable topographically
UV bright	UV dark
dark in visible	bright in visible
1 μm band anti-correlated with albedo, suggesting space weathering	deep 1 μm band indicating little space weathering
Pyroxenes similar to eucrite/howardite meteorites	Pyroxenes similar to eucrite/howardite meteorites, plus olivine, plus material similar to diogenite meteorites

Figure Captions.

Figure 1. Spatial variations in Vesta's UV brightness. All figures display flux units of $\text{ergs/cm}^2\text{-sec-}\text{\AA}$. a) 2700-2800 \AA ; b) 2800-2900 \AA ; c) 2900-3000 \AA ; d) 3000-3100 \AA . The spectral reflectance curves of the two boxed points in (c) are shown in Fig. 4. The right portion of each plot is the eastern hemisphere.

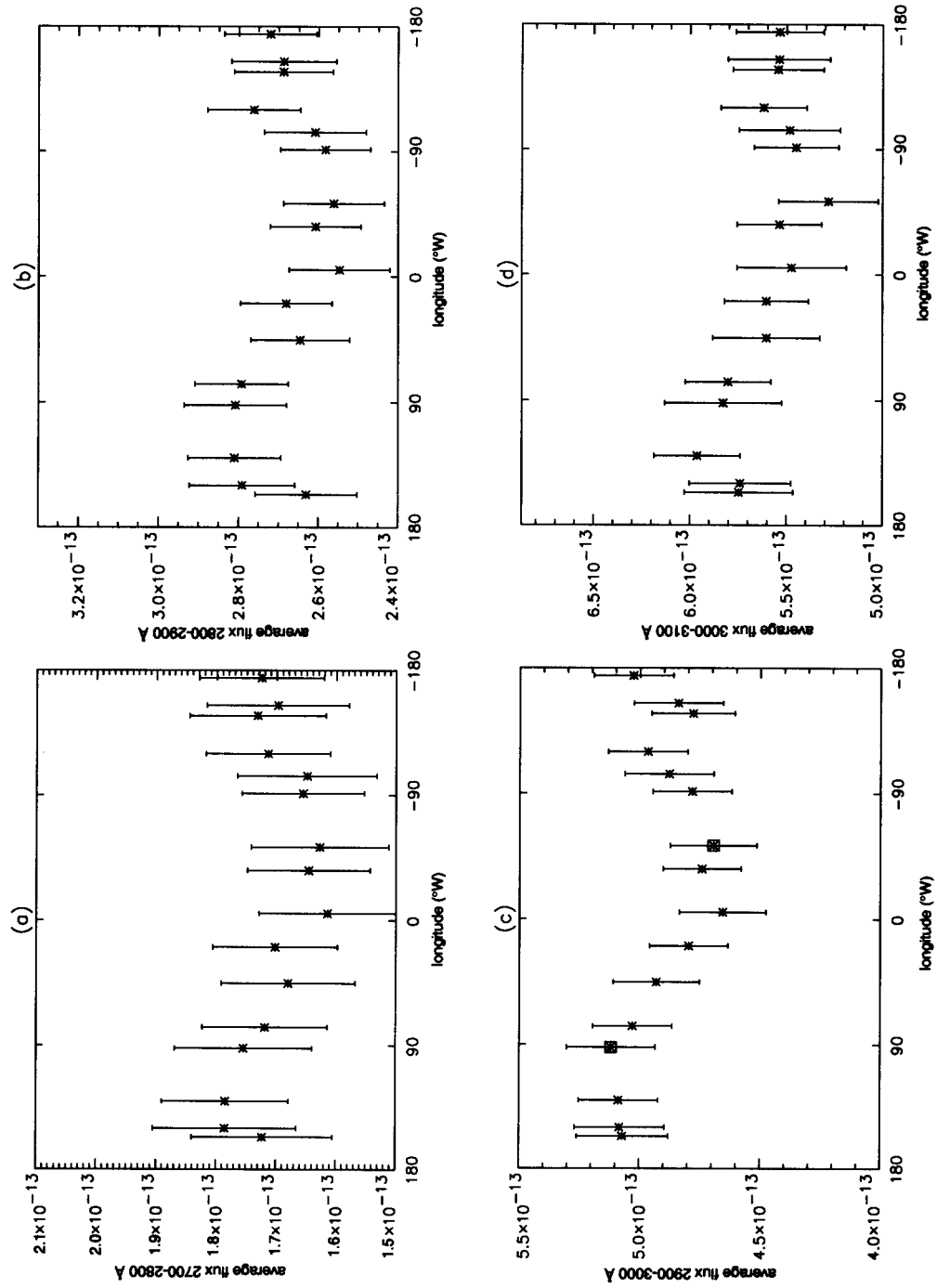
Figure 2. a) Spectral reflectance (at 17° solar phase angle) of two regions on Vesta, with spectral models overplotted. The triangles represent the reflectance measured at 92°W (LWP 18955); asterisks represent the reflectance measured at -52°W (LWP 18952). The locations of these two observations are also indicated in Fig. 1c. Small-scale spectral features are due to mismatches in solar spectrum. Spectra have been smoothed and binned into 11 \AA bins. The western hemisphere model (dashed line) includes 83% aubrite and 17% diogenite, while the model to the eastern hemisphere (solid line) includes 90% aubrite and 10% fayalite. b) Model fits extending to visible wavelengths.

Figure 3. a) Reflectance curves as in Fig 2a. The western hemisphere model (dashed line) includes 90% howardite and 310% diogenite, while the model to the eastern hemisphere (solid line) includes 54% howardite, 36% diogenite and 10% fayalite. b) Model fits extending to visible wavelengths, demonstrating a spectral reversal similar to that seen on Vesta.

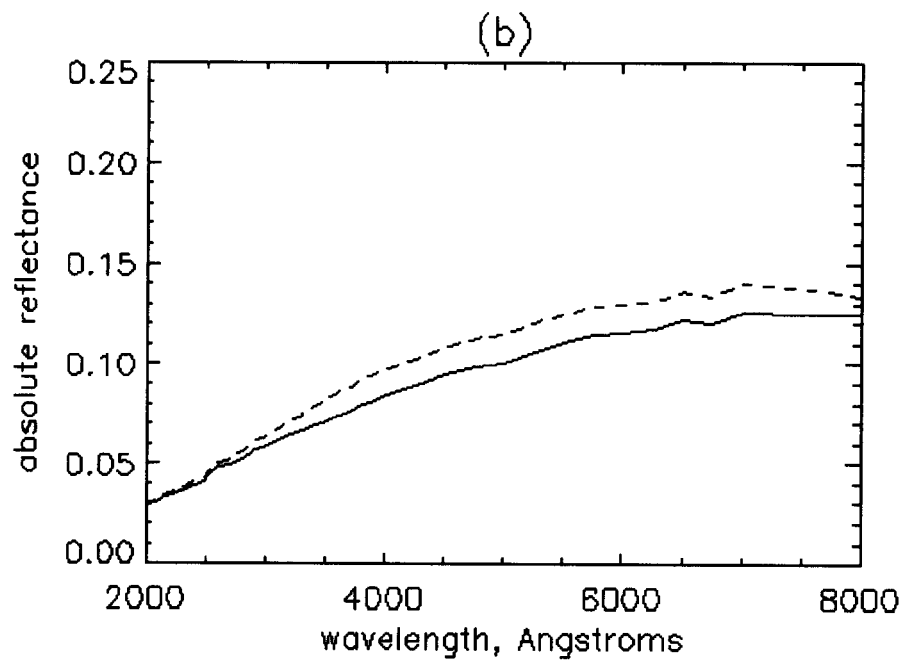
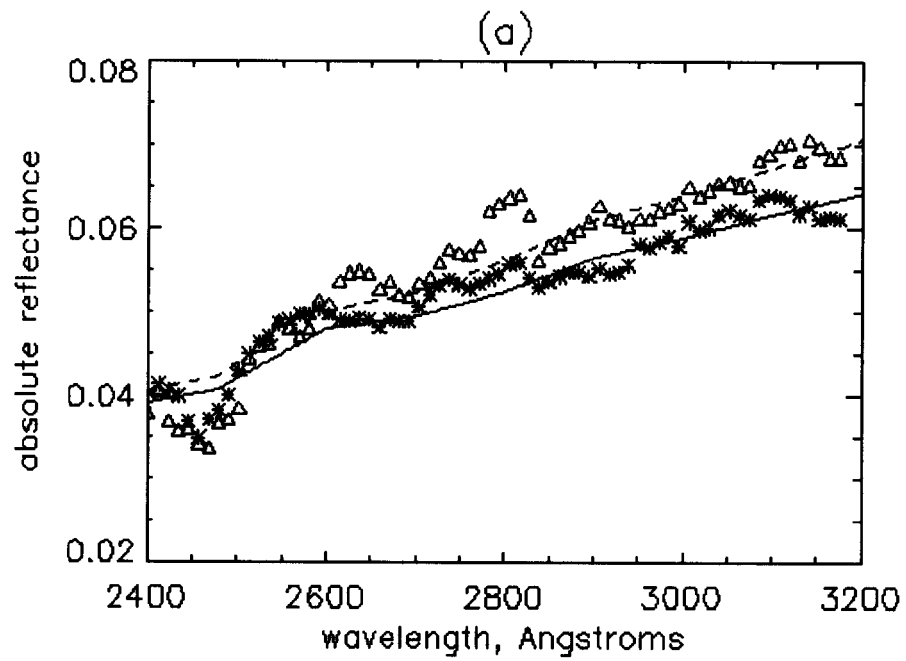
Figure 4a. Topographic map of Vesta from Thomas *et al.* (1997b). The right portion of the map is the eastern hemisphere.

Figure 4b. Projection of topographic map on Vesta shape model centered at 20°S for several longitudes. Dynamic heights cover ± 12 km (see Thomas *et al.*, 1997b). See Fig. 2a for color bar.

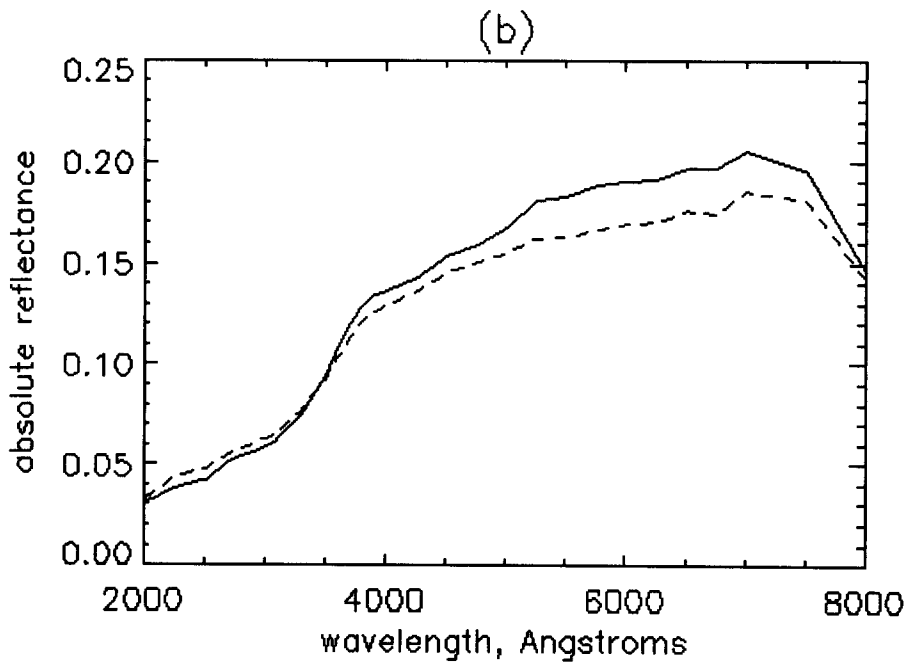
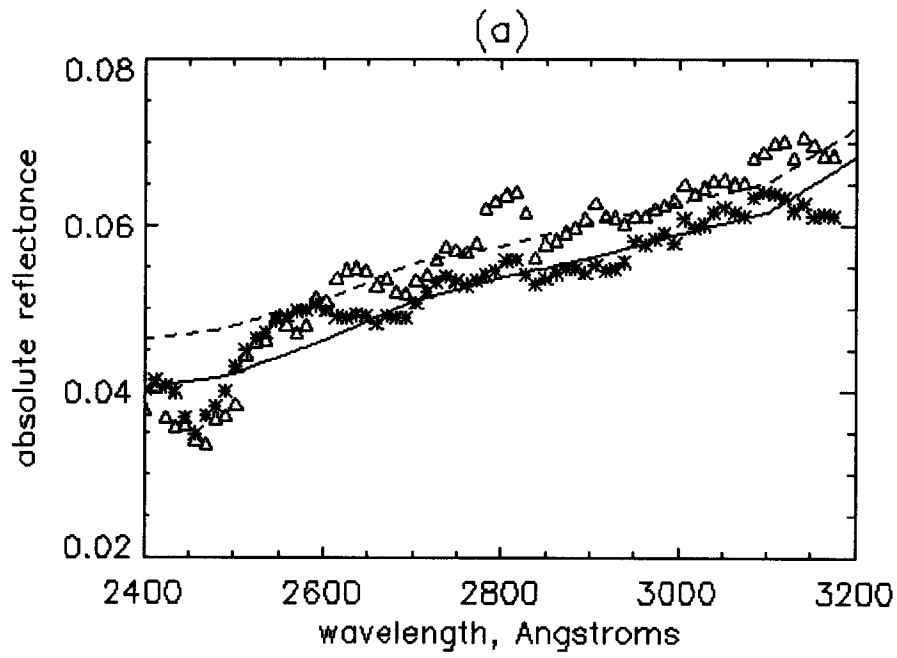
Hendrix *et al.* Fig. 1



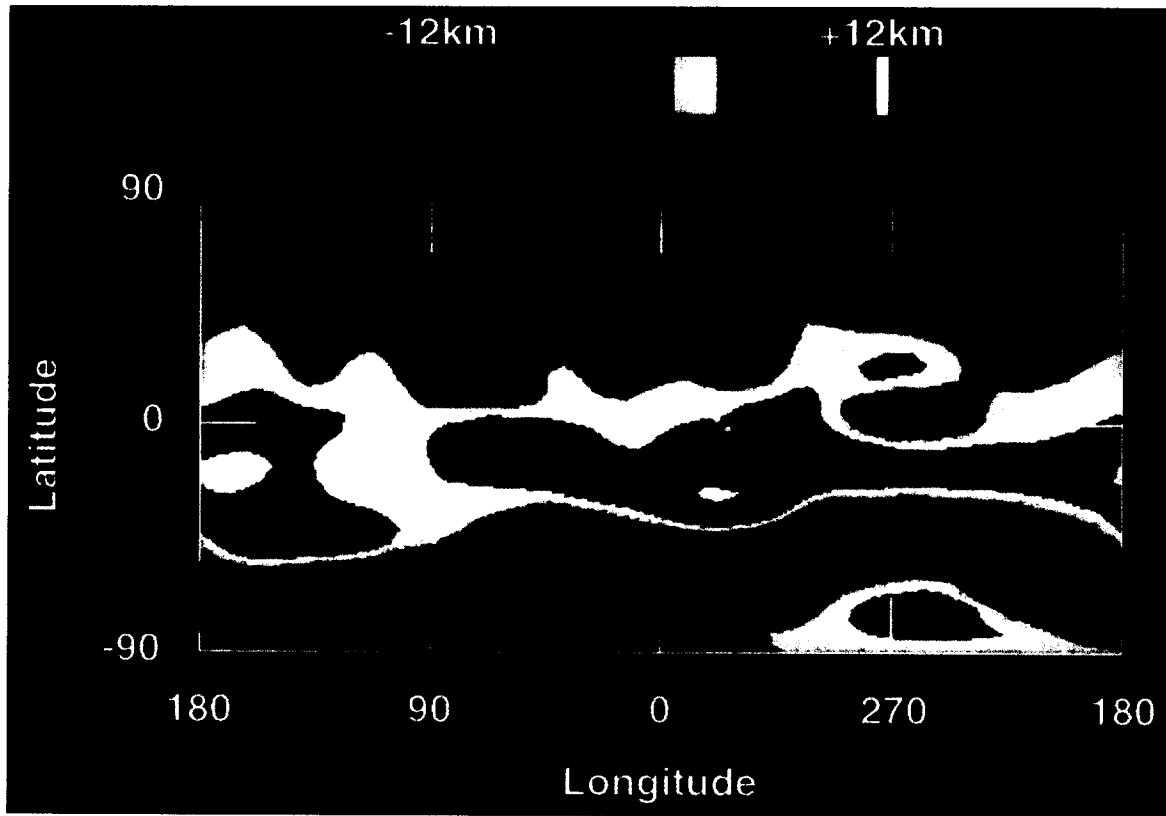
Hendrix *et al.* Fig. 2



Hendrix *et al.* Fig. 3



Hendrix *et al.* Fig. 4a



Hendrix *et al.* Fig. 4b

